MEMS Switched Tunable Inductors

Mina Rais-Zadeh, *Student Member, IEEE*, Paul A. Kohl, *Member, IEEE*, and Farrokh Ayazi, *Senior Member, IEEE*

***Abstract*—This paper presents a new implementation of integrated tunable inductors using mutual inductances activated by micromechanical switches. To achieve a large tuning range and a high quality factor, silver was used as the structural material, and silicon was selectively removed from the backside of the substrate. Using this method, a maximum tuning of 47% at 6 GHz is achieved for a 1.1 nH silver inductor fabricated on a low-loss polymer membrane. The effect of the quality factor on the tuning characteristic of the inductor is investigated by comparing the measured result of identical inductors fabricated on various substrates. To maintain the quality factor of the silver inductor, the device was encapsulated using a low-cost wafer-level polymer packaging technique. [2007-0118]**

***Index Terms*—Inductors, micromachining, quality factor, switches, tunable inductor, tuning.**

I. Introduction

TUNABLE inductors can find application in frequency-agile radios, tunable filters, voltage-controlled oscillators, and reconfigurable impedance matching networks. The need for tunable inductors becomes more critical when optimum tuning or impedance matching in a broad frequency range is desired. Both discrete and continuous tuning of passive inductors using micromachining techniques have been reported in the literature [1]–[5]. Discrete tuning of inductors is usually achieved by changing the length or configuration of a transmission line using micromachined switches [6], [7]. The incorporation of switches in the body of the tunable inductor increases the resistive loss and, hence, reduces the quality factor (Q). Alternatively, continuous tuning of inductors is realized by displacing a magnetic core [1], [4], [8], changing the permeability of the core [9], or using movable structures with large traveling range [1]–[3]. Although significant tuning has been reported using these methods, the fabrication or the actuation techniques are complex, making the on-chip implementation difficult. In addition, the Q value of the reported tunable inductors is not high enough for many wireless and RF integrated circuit applications [9], [10].

The objective of this paper is to implement small form-factor high-Q switched tunable inductors for the 1–10-GHz frequency range. In this frequency range, the permeability of most magnetic materials degrade [2], [11], making them unsuitable for our application. In addition, small displacement is preferred to simplify the encapsulation process of a tunable inductor. We have developed tunable inductors based on transformer action using on-chip micromachined vertical switches with an actuation gap of a few micrometers. We use silver (Ag) because it has the highest electrical conductivity and a low Young's modulus compared to other metals. To encapsulate the tunable inductors, we employ a wafer-level polymer packaging technique. The full fabrication process is simple and requires six lithography steps, including the packaging steps, and is post CMOS compatible. Using this process, a 1.1 nH silver tunable inductor is switched to four discrete values and shows a maximum tuning of 47% at 6 GHz. This inductor exhibits an embedded Q in the range of 20–45 at 6 GHz and shows no degradation in Q after packaging. The switched tunable inductor presented here outperforms the reported tunable inductors with respect to its high embedded quality factor at radio frequencies (1–10 GHz).

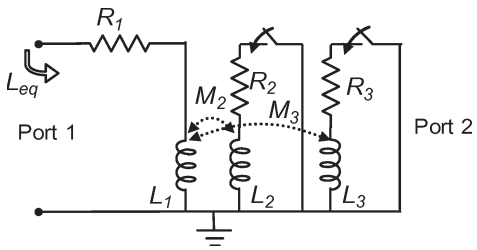

Fig. 1. Switched tunable inductor electrical model.

II. Design

Fig. 1 shows the schematic view of the switched tunable inductor [12]. The inductance is taken from port one, and a plurality of inductors at port two (secondary inductors) are switched in and out (two inductors in this case). When all switches at port two are open, the inductance seen from port one is L_1. Inductors at port two are different in size and, thus, have different mutual inductance effect on port one when activated. The effective inductance of port one can have $1 + n(n+1)/2$ different states, where n is the number of inductors at port two. In the case of two inductors at port two, four discrete values can be achieved.

The equivalent inductance and series resistance seen from port one are found from

$$L_{\rm eq} = L_1 \left(1 - \sum_{i=2}^{n+1} \frac{b_i k_i^2 L_i^2 \omega^2}{R_i^2 + L_i^2 \omega^2}\right), \qquad b_i = 0 \text{ or } 1 \quad (1)$$

$$R_{\rm eq} = R_1 + \sum_{i=2}^{n+1} \frac{b_i R_i k_i^2 L_1 L_i \omega^2}{R_i^2 + L_i^2 \omega^2}, \qquad b_i = 0 \text{ or } 1 \quad (2)$$

Manuscript received May 22, 2007; revised August 27, 2007. This work was supported by the National Science Foundation. Subject Editor D. Cho.

M. Rais-Zadeh and F. Ayazi are with the Department of Electrical and Computer Engineering, Georgia Institute of Technology, Atlanta, GA 30332-0250 USA (e-mail: minaii@ece.gatech.edu; ayazi@ece.gatech.edu).

P. A. Kohl is with the Department of Chemical and Biomolecular Engineering, Georgia Institute of Technology, Atlanta, GA 30332-0100 USA (e-mail: Paul.Kohl@chbe.gatech.edu).

Color versions of one or more of the figures in this paper are available online at http://ieeexplore.ieee.org.

Digital Object Identifier 10.1109/JMEMS.2007.910257

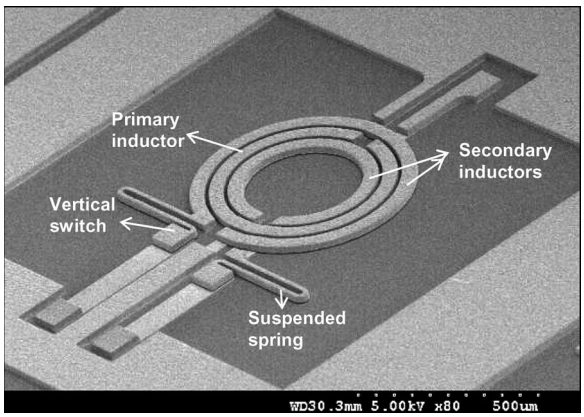

Fig. 2. SEM view of a 20 μm-thick silver switched tunable inductor fabricated on an Avatrel membrane.

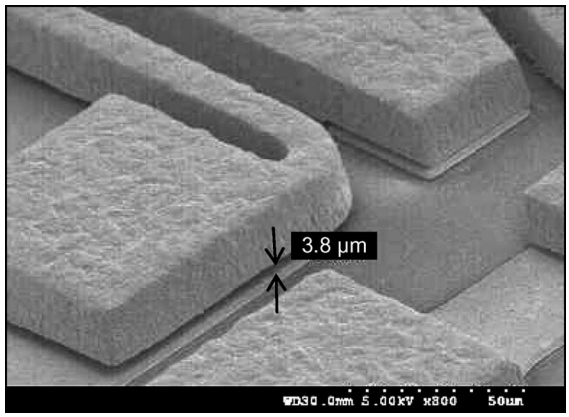

Fig. 3. Close-up SEM views of the switch, showing the actuation gap.

where L_i is the inductance value of the secondary inductors, R_i represents the series resistance of each secondary inductor plus the contact resistance of its corresponding switch, k_i is the coupling coefficient, b_i represents the state of the switch and is 1 (or 0) when the switch is on (or off), and ω is the angular frequency. The largest change in the effective inductance occurs when all switches at port two are on. In this case, the percentage tuning can be found from

$$\%\ \text{tuning} = \sum_{i=2}^{n+1} \frac{b_i k_i^2 L_i^2 \omega^2}{(R_i^2 + L_i^2 \omega^2)} \times 100. \tag{3}$$

From (3), it can be seen that to achieve large tuning, R_i should be much smaller than the reactance of the secondary inductors $(L_i\omega)$, which requires high-Q inductors and low-contact-resistance switches that are best implemented using micromachining technology. For this reason, we used silver, which has the highest electrical conductivity of all materials at room temperature, to implement high-Q inductors and micromachined ohmic switches. The switches are actuated by applying a direct-current voltage to port two. The use of silver also offers the advantage of having a smaller tuning voltage compared to other high-conductivity metals (e.g., copper) because of its lower Young's modulus.

Fig. 2 shows the SEM view of a switched tunable silver inductor. The two inductors at port two are in series connection with a vertical ohmic switch through a narrow spring. Springs are designed to have a small series resistance and stiffness < 15 N/m. The actuation voltage of the vertical switch with an actuation gap of 3.8 μm is 40 V. This voltage can be reduced to less than 5 V by reducing the gap size to $\sim$0.9 μm. The close-up view of the switch, showing the actuation gap, is shown in Fig. 3.

III. Fabrication

The schematic diagram of the fabrication process flow is shown in Fig. 4.

The substrate was first spin coated with a 20 μm-thick low-loss polymer, Avatrel (Promerus, LLC, Brecksville, OH 44141). The routing metal layer was then formed by evaporating a 2 μm-thick silver layer. A thin layer ($\sim$100 Å) of

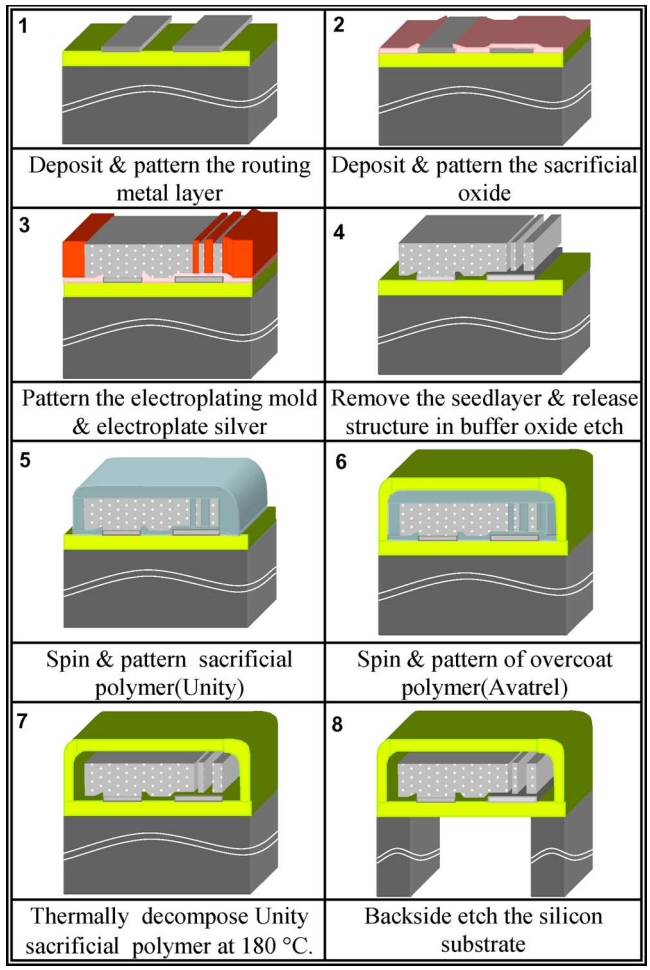

Fig. 4. Packaged switched tunable inductor fabrication process.

titanium (Ti) was used to promote the adhesion between the silver and Avatrel layers. The actuation gap was then defined by depositing a 3.8 μm-thick plasma-enhanced chemical vapor deposited (PECVD) sacrificial silicon dioxide layer at 160 °C. The deposition temperature of silicon dioxide was reduced to preserve the quality of the Avatrel layer, which provides mechanical support for the released device. The inductors and the switches were formed by electroplating silver onto a 20 μm-thick photoresist mold [13]. A thin layer of Ti/Ag/Ti (100 Å/

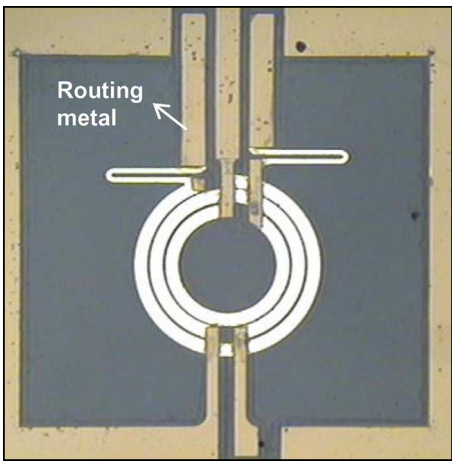

Fig. 5. Micrograph of the switched Ag inductor, taken from the backside of the Avatrel membrane.

300 Å/100 Å) was sputter deposited and served as the seed layer for plating. The top titanium layer prevents the electroplating of silver underneath the electroplating mold and was dry etched from the open areas in a reactive ion etching (RIE) system. The use of the Ti layer is especially important when the distance between the silver lines is less than 10 μm.

The plating bath consisted of 0.35 mol/L of potassium silver cyanide (KAgCN) and 1.69 mol/L of potassium cyanide (KCN). A current density of 1 mA/cm^2 was used in the plating process. The electroplating mold was subsequently removed. The seed layer was removed using a combination of a wet and a dry etching process. Compared to the sputtered silver, the electroplated silver layer has a larger grain size, resulting in a higher wet etch rate using an H_2O_2 : NH_4OH solution. The hydrogen peroxide oxidizes the silver and the ammonium hydroxide solution complexes and dissolves the silver ions. When wet etched, the thick high-aspect-ratio lines of the electroplated silver get etched much faster than the sputtered seed layer that is between the walls of the thick electroplated silver. Dry etching of silver, on the other hand, decouples the oxidation and dissolution steps, resulting in almost the same removal rate for the small-grained sputtered layer as the large-grained plated silver. The silver was first oxidized in an oxygen plasma (dry etch), and then, the silver oxide layer was dissolved in dilute ammonium hydroxide solution. Using this etching method, the seed layer was removed without loosing excess electroplated silver. The device was then released in dilute buffer oxide etch. The released device was then wafer-level packaged [14]. A thermally decomposable sacrificial polymer, Unity (Promerus LLC, Brecksville, OH 44141), was applied and patterned. Then, the overcoat polymer (Avatrel), which is thermally stable at the Unity decomposition temperature, was spin coated and patterned. Finally, the Unity sacrificial polymer was decomposed at 180 °C. The loss of silicon substrate was eliminated by selective backside etching of the silicon underneath the device, leaving a polymer membrane under the device. A micrograph of an unpackaged inductor, taken from the backside of the Avatrel membrane, is shown in Fig. 5. The highest processing temperature, including the packaging steps, is 180 °C, and thus, the process is post CMOS compatible.

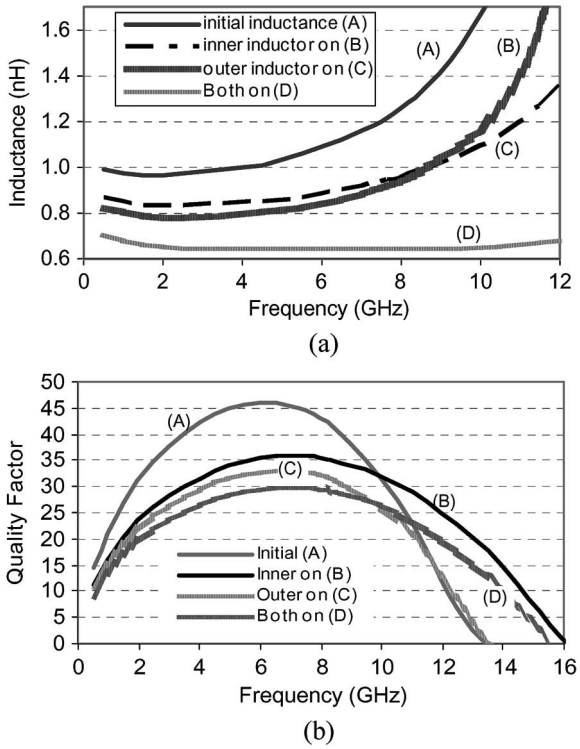

Fig. 6. Simulated (a) inductance and (b) Q of the switched tunable inductor on the Avatrel membrane, showing a maximum tuning of 47.5% at 6 GHz.

IV. Discussion

A. Simulation Results

The tunable inductors were simulated in the Sonnet electromagnetic tool. Fig. 6 shows the simulated effective inductance and Q seen from port one at four states of the tunable inductor [state (A) is when all the switches are off]. As shown in Fig. 6(a), a maximum inductance change of 47% is expected at the frequency of the peak Q, when both switches are on. At low frequencies, R_i is not negligible compared to $L_i\omega$, and according to (3), the percent tuning is small. At higher frequencies, $L_i\omega \gg R_i$ [2] and magnetic coupling is stronger. Therefore, the amount of tuning increases at higher frequencies. The outer inductor is larger in size than the inner one, and its peak $Q(L_i\omega/R_i)$ occurs at lower frequencies. As a result, the outer inductor has a larger effect on the effective inductance at lower frequencies. In contrast, the frequency of the peak Q for the inner inductor is higher. Thus, it has a larger effect at this frequency range.

B. Measurement Results

Several switched tunable inductors were fabricated and tested. On-wafer S-parameter measurements were carried out using an *hp*8510C VNA and Cascade GSG microprobes. The pad parasitics is not de-embedded. The test setup is schematically shown in Fig. 7. Each switched tunable inductor was tested several times to ensure repeatability of the measurements.

Fig. 8 shows the measured inductance of a switched silver inductor fabricated on an Avatrel membrane. The inductance

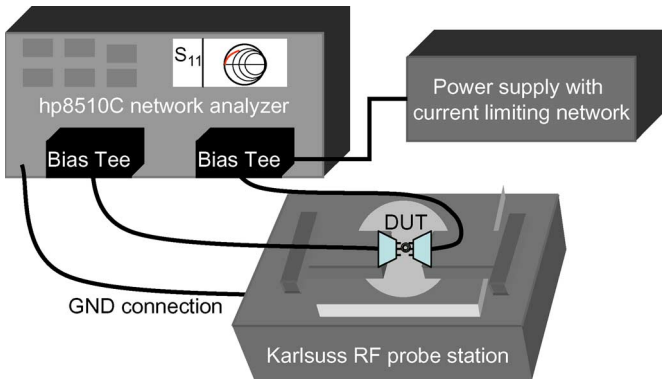

Fig. 7. Schematic of the test setup.

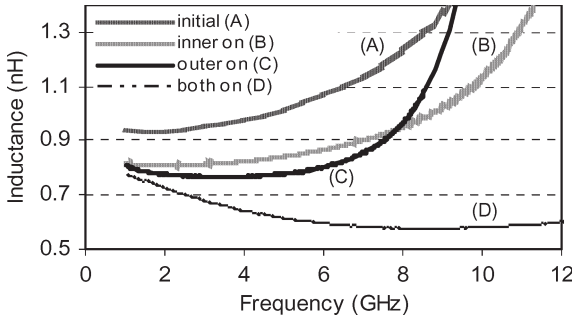

Fig. 8. Measured inductance showing a maximum tuning of 47% at 6 GHz when both inductors are on.

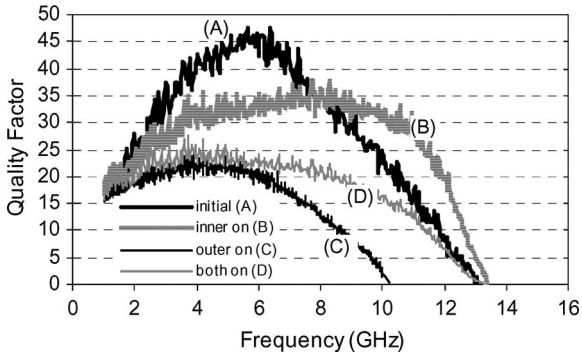

Fig. 9. Measured embedded Q, showing the Q drops as the inductor is tuned.

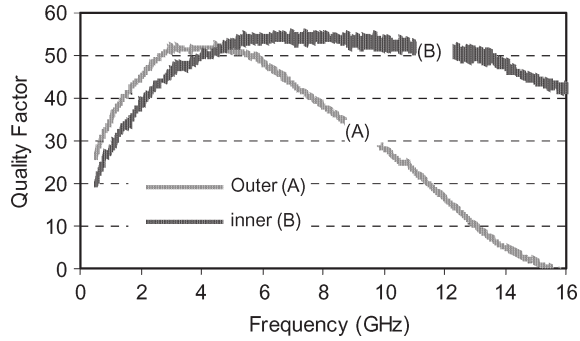

Fig. 10. Measured Q of the inductors at port two on the Avatrel membrane.

is switched to four different values and is tuned from 1.1 nH at 6 GHz to 0.54 nH, which represents a maximum tuning of 47% at 6 GHz. The maximum tuning was achieved when both inductors were switched on. At 6 GHz, the effective inductance drops to 0.79 nH when the outer inductor is on and to 0.82 nH when the inner inductor is on. The measured results are in good agreement with the simulated response shown in Figs. 6 and 8. The measured embedded Q of this inductor in different states is shown in Fig. 9. As shown, the inductor exhibits a peak Q of 45 when the inductors at port two are both off. The Q drops to 20 when both switches are on. The drop of Q is consistent with (2). When any of the inductors at port two are switched on, $L_{\rm eq}$ decreases while the effective resistance increases, resulting in a drop in Q as the inductor is tuned. Fig. 10 shows the measured Q of the inductors at port two. From Fig. 10, it can be seen that the peak Q of the inner inductor is at frequencies $>$ 7 GHz. Thus, the maximum change in the effective inductance, resulting from switching on the inner inductor, occurs at this frequency range (Fig. 8).

C. Effect of Q on Tuning

To demonstrate the effect of the quality factor on the tuning ratio of the switched tunable inductors, identical devices were fabricated on different substrates. On sample A, inductors were fabricated on a CMOS-grade silicon substrate passivated with a 20 μm-thick PECVD silicon dioxide layer. The silicon substrate was removed from the backside of inductors of sample B, leaving behind a 20 μm-thick silicon dioxide membrane beneath the inductors. Silicon dioxide has a loss tangent higher than that of Avatrel, which results in a higher substrate loss [15]. Therefore, the Q value of the inductors on the silicon dioxide membrane (sample B) is lower than that of the inductors on the Avatrel membrane shown in Fig. 9.

Fig. 11 compares the effective inductance and Q of the tunable inductors on samples A and B at two different states.

As shown in Fig. 11, the percent tuning is lower for sample A, which has a lower Q. The inductance of sample A changes by 36.8% at 4.7 GHz when the outer inductor is switched on (state A$'$). At this frequency, the tuning that results from switching on the outer inductor of sample B (state B$'$) is only 9.7%. Consequently, employing low-loss materials such as Avatrel helps improve the tuning characteristic of the switched tunable inductors.

It should be mentioned that the performance of these tunable inductors can be improved further. The routing metal layer of the fabricated inductors is less than three times the skin depth of silver at low frequencies, where the metal loss is the dominant Q-limiting mechanism. Therefore, the quality factor of the switched tunable inductors is limited by the metal loss of the routing layer and can be improved by increasing the thickness of this layer. A fixed inductor with identical dimension to L_1 but with no routing layer exhibits a record-high embedded Q of $>$ 150 at 6 GHz [13], as shown in Fig. 12. An SEM view of this inductor is shown in Fig. 13. The limited thickness of the routing layer has a more pronounced effect on the Q of the switching inductors at port two, as the length of this layer is longer at port two (as shown in Fig. 2). The Q of a 0.88 nH inductor with identical dimensions to the inner inductor but with no routing layer is shown in Fig. 14. This inductor, without routing, exhibits a high embedded Q of $>$ 140 at 6 GHz.

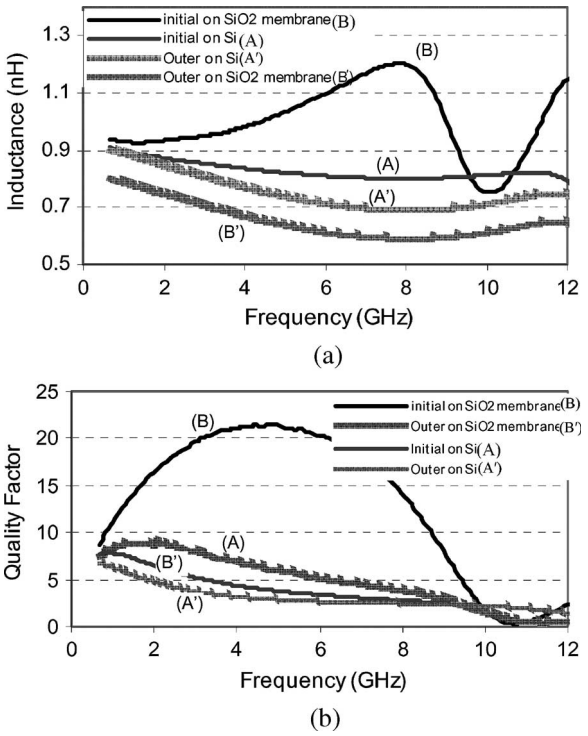

Fig. 11. Measured (a) inductance and (b) embedded Q of identical tunable inductors fabricated on (A) a passivated silicon substrate and (B) a 20 μm-thick silicon dioxide membrane.

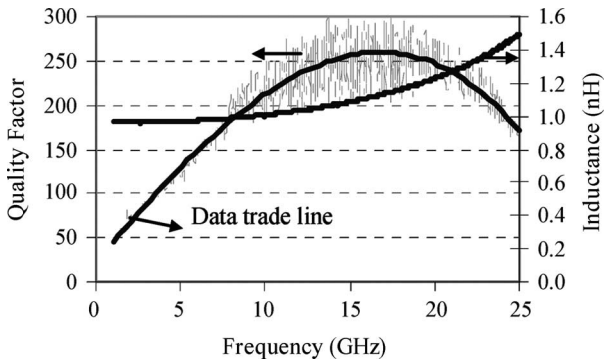

Fig. 12. Measured Q and inductance of a one-turn 1 nH inductor on the Avatrel membrane, showing Q in excess of 120 at frequencies above 5 GHz.

Comparing Figs. 10 and 14 reveals that the metal loss is twice as much for the inner inductor with the thin routing layer.

D. Packaging Results

Hermetic or semihermetic sealing of silver microstructures increases the lifetime of the silver devices by decreasing its exposure to the corrosive gases and humidity. Silver is very sensitive to hydrogen sulfide (H_2S), which forms silver sulfide (Ag_2S), even at a very low concentration of corrosive gas [16]. The decomposition of the contact surfaces leads to an increase of the surface resistance and, hence, to a lower Q and, for tunable inductors, a lower tuning range. Another problem that impedes the wide application of silver is electrochemical migration, which occurs in the presence of wet surface and applied bias. Silver migration usually occurs between adjacent

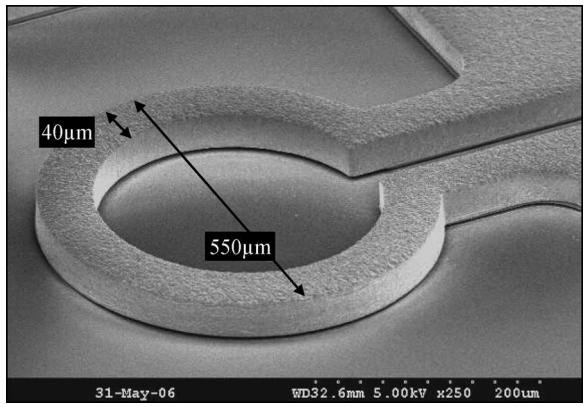

Fig. 13. SEM view of the primary inductor without the routing layer. This inductor exhibits $Q > 140$ at 6 GHz.

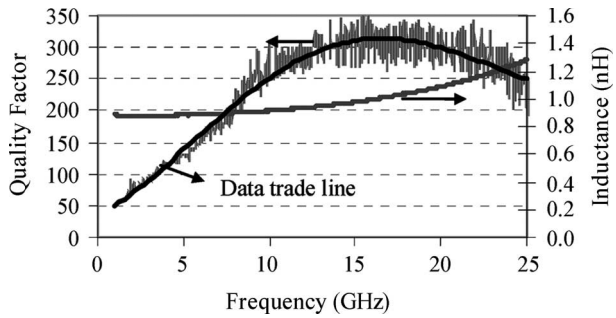

Fig. 14. Measured Q and inductance of the inner inductor without the routing layer, fabricated on an Avatrel membrane, showing Q in excess of 140 at 6 GHz.

conductors/electrodes, which leads to the formation of dendrites and finally results in an electrical short-circuit failure. The failure time is related to the relative humidity, temperature, and the strength of the electric field [17]. For the tunable inductor structure presented here, the possible location of failure is between the switch pads only when the switch is in contact. When off, there is an air gap between the switch pads, which blocks the path for the growth of dendrites.

In this paper, we incorporated a semihermetic packaging technique to prevent or lessen their exposure to the corrosive gases and to encapsulate the tunable inductor. The preliminary results of the packaging techniques are reported here. If necessary, subsequent overmolding can provide additional strength and resilience and ensures long-term hermeticity. Fig. 15 is the SEM view of the packaged switched tunable inductor and the close-up view of a broken package, showing the air cavity inside. The inductor trace was peeled during the cleaving process.

Fig. 16 shows the Q of two identical inductors before decomposition of the Unity sacrificial polymer. The two inductors, one packaged and one unpackaged, were fabricated on a silicon-nitride-passivated high-resistivity $(\rho = 1\ \text{k}\Omega \cdot \text{cm})$ silicon substrate. As expected, the undecomposed packaged inductor has a lower Q at higher frequencies because of the dielectric loss of the Unity sacrificial polymer. When Unity was decomposed and the packaging process was completed, the two inductors were, again, measured. As shown in Fig. 17, the switched tunable inductor showed no degradation in Q after

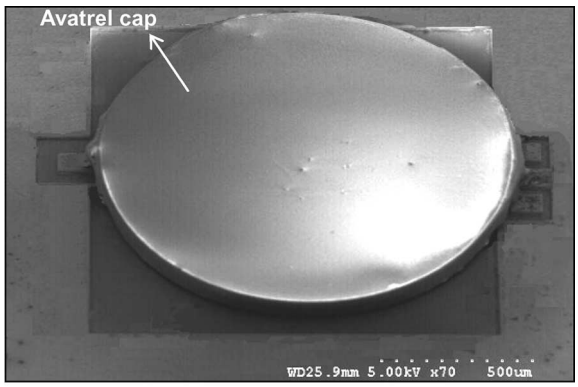

(a)

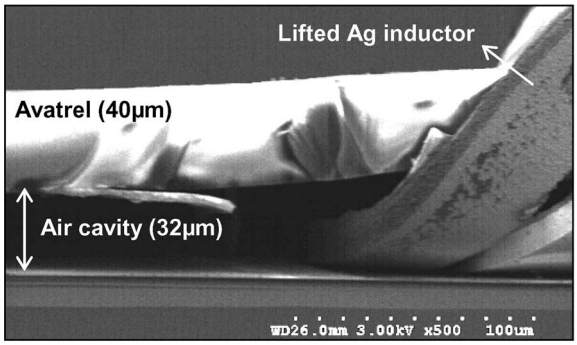

(b)

Fig. 15. (a) SEM view of the packaged switched inductor and (b) close-up view of a broken package.

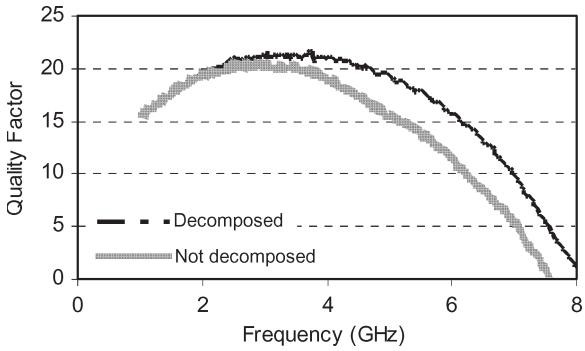

Fig. 16. Measured embedded Q of two identical inductors before decomposition, one packaged and one unpackaged.

packaging, indicating that the Unity polymer was fully decomposed. To demonstrate the effect of packaging on preserving the Q of the silver tunable inductor, the performance of the packaged inductor was measured after 10 months and is shown in Fig. 18. The performance of the packaged inductor has not changed during this period.

V. Conclusion

The implementation and characterization results of high-performance switched tunable silver inductors using a fully CMOS-compatible process have been presented. A 1.1 nH inductor was switched to four discrete values and showed a tuning of 47% at 6 GHz. The effect of Q on the tuning characteristic of the inductor has been demonstrated. Wafer-level polymer packaging of the tunable inductor did not cause any additional loss, and the performance of the packaged silver inductor did not change after 10 months.

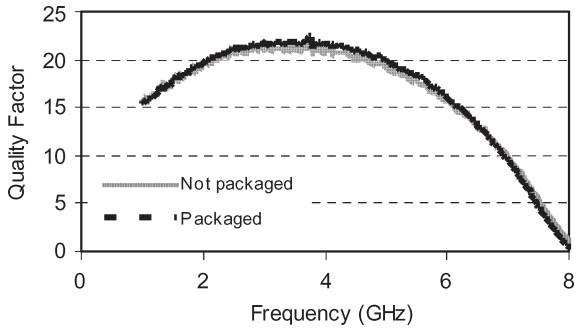

Fig. 17. Measured embedded Q of two identical inductors when both switches are off, one package and one unpackaged.

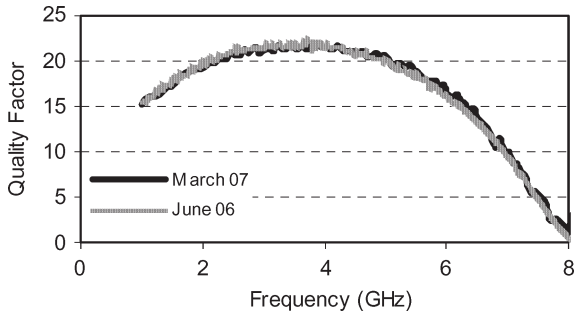

Fig. 18. Measured embedded Q of the packaged silver tunable inductor, showing no degradation in Q after 10 months.

Acknowledgment

The authors would like to thank the staff at the Georgia Tech Microelectronics Research Center for their assistance.

References

[1] W. P. Shih, Z. Li, D. T. McCormick, N. C. Tien, and C. Y. Hui, "Tunable solenoid microinductors utilizing permalloy electro-thermal vibromotors," in *Proc. IEEE Int. Conf. Microelectromech. Syst.*, Maastricht, The Netherlands, Jan. 2004, pp. 793–796.

[2] C. M. Tassetti, G. Lissorgues, and J. P. Gilles, "Tunable RF MEMS microinductors for future communication systems," in *Proc. IEEE MTT-S*, Philadelphia, PA, Jun. 2003, vol. 3, pp. 541–545.

[3] I. Zine-El-Abidine, M. Okoniewski, and J. G. McRory, "RF MEMS tunable inductor," in *Proc. IEEE Microw., Radar Wireless Conf.*, Warsaw, Poland, May 2004, vol. 3, pp. 817–819.

[4] S. Chang and S. Sivoththaman, "A tunable RF MEMS inductor on silicon incorporating an amorphous silicon bimorph in a low-temperature process," *IEEE Electron Device Lett.*, vol. 27, no. 11, pp. 905–907, Nov. 2006.

[5] D. R. Pehlke, A. Burstein, and M. F. Chang, "Extremely high-Q tunable inductor for Si-based RF integrated circuit applications," in *IEDM Tech. Dig.*, Washington, DC, Dec. 1997, pp. 63–66.

[6] P. Park, C. S. Kim, M. Y. Park, S. D. Kim, and H. K. Yu, "Variable inductance multilayer inductor with MOSFET switch control," *IEEE Electron Device Lett.*, vol. 25, no. 3, pp. 144–146, Mar. 2004.

[7] S. Lee, J. M. Kim, J. M. Kim, Y. K. Kim, and Y. Kwon, "Millimeter-wave MEMS tunable low pass filter with reconfigurable series inductors and capacitive shunt switches," *IEEE Microw. Wireless Compon. Lett.*, vol. 15, no. 10, pp. 691–693, Oct. 2005.

[8] J. Salvia, J. A. Bain, and C. P. Yue, "Tunable on-chip inductors up to 5 GHz using patterned permalloy laminations," in *IEDM Tech. Dig.*, Washington, DC, Dec. 2005, pp. 943–946.

[9] M. Vroubel, Y. Zhuang, B. Rejaei, and J. N. Burghartz, "Integrated tunable magnetic RF inductor," *IEEE Electron Device Lett.*, vol. 25, no. 12, pp. 787–789, Dec. 2004.
[10] N. Sarkar, D. Yun, M. Ellis, E. Horne, J. B. Lee, H. Lu, R. Mansour, A. Nallani, and G. Skidmore, "Microassembled tunable MEMS inductor," in *Proc. IEEE Int. Conf. Microelectromech. Syst.*, Miami, FL, Jan. 2005, pp. 183–186.
[11] D. Gardner, A. M. Crawford, and S. Wang, "High frequency (GHz) and low resistance integrated inductors using magnetic materials," in *Proc. IEEE Int. Interconnect Technol. Conf.*, Burlingame, CA, Jun. 2001, pp. 101–103.
[12] M. Rais-Zadeh, P. A. Kohl, and F. Ayazi, "A packaged micromachined switched tunable inductor," in *Proc. IEEE Int. Conf. Microelectromech. Syst.*, Kobe, Japan, Jan. 2007, pp. 799–802.
[13] M. Rais-Zadeh, P. A. Kohl, and F. Ayazi, "High-Q micromachined silver passives and filters," in *IEDM Tech. Dig.*, San Francisco, CA, Dec. 2006, pp. 727–730.
[14] P. Monajemi, P. Josef, P. A. Kohl, and F. Ayazi, "A low-cost wafer-level packaging technology," in *Proc. IEEE Int. Conf. Microelectromech. Syst.*, Miami, FL, Jan. 2005, pp. 634–637.
[15] M. Rais-Zadeh and F. Ayazi, "Characterization of high-Q spiral inductors on thick insulator-on-silicon," *J. Micromech. Microeng.*, vol. 15, no. 11, pp. 2105–2112, Nov. 2005.
[16] B. Chunovsky, D. L. Swindler, and J. R. Thompson, "A touch of gray," *IEEE Ind. Appl. Mag.*, vol. 8, no. 5, pp. 45–52, Sep./Oct. 2002.
[17] R. Manepalli, F. Stepniak, S. A. Bidstrup-Allen, and P. A. Kohl, "Silver metallization for advanced interconnects," *IEEE Trans. Adv. Packag.*, vol. 22, no. 1, pp. 4–8, Feb. 1999.

Mina Rais-Zadeh (S'03) received the B.S. degree in electrical engineering from Sharif University of Technology, Tehran, Iran, in 2002, and the M.S. degree in electrical and computer engineering from Georgia Institute of Technology, Atlanta, in 2005, where she is currently working toward the Ph.D. degree, with a focus on the design and fabrication of wafer-level packaged high-performance tunable passives and bandpass filters.

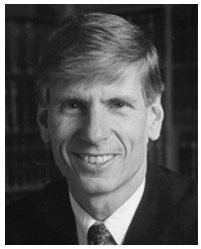

Paul A. Kohl (A'92–M'03) received the Ph.D. degree in chemistry from The University of Texas, Austin, in 1978.

He is with Georgia Institute of Technology (Georgia Tech), Atlanta, as a Regents' Professor of chemical engineering. He was with AT&T Bell Laboratories from 1978 to 1989. At Bell Laboratories, he was involved in new materials and processing methods for semiconductor devices. In 1989, he joined the faculty of Georgia Tech. His research interests include ultra-low-k dielectric materials, interconnects for microelectronic devices, and electrochemical energy conversion devices. He has more than 150 journal publications. He is the holder of 40 patents.

Farrokh Ayazi (S'96–M'99–SM'05) received the B.S. degree in electrical engineering from the University of Tehran, Tehran, Iran, in 1994 and the M.S. and Ph.D. degrees in electrical engineering from the University of Michigan, Ann Arbor, in 1997 and 2000, respectively.

He joined the faculty of Georgia Institute of Technology, Atlanta, in December 1999, where he is currently an Associate Professor in the School of Electrical and Computer Engineering. His research interests are integrated microelectromechanical and nanoelectromechanical resonators, IC design for MEMS and sensors, RF MEMS, inertial sensors, and microfabrication techniques.

Prof. Ayazi is the recipient of the 2004 National Science Foundation CAREER Award, the 2004 Richard M. Bass Outstanding Teacher Award, and the Georgia Tech College of Engineering Cutting Edge Research Award for 2001–2002. He received a Rackham Predoctoral Fellowship from the University of Michigan for 1998–1999. He is an Editor of the JOURNAL OF MICROELECTROMECHANICAL SYSTEMS and serves on the Technical Program Committees of the IEEE International Solid State Circuits Conference and the International Conference on Solid State Sensors, Actuators and Microsystems (Transducers).